Chapter 7

Multidimensional Correlation Spectroscopy by Covariance NMR

David A. Snyder[1] and Rafael Brüschweiler[2]

[1]*Department of Chemistry, William Paterson University, 300 Pompton Road, Wayne, NJ 07470, USA*
[2]*Chemical Sciences Laboratory, Department of Chemistry and Biochemistry & National High Magnetic Field Laboratory, Florida State University, Tallahassee, FL 32306, USA*

7.1 INTRODUCTION

Covariance nuclear magnetic resonance (NMR) spectroscopy encompasses methods that establish correlations between nuclear magnetic spins by means of statistical covariances.[1–3] The covariance transform serves as a complement to, or replacement of, the Fourier transform (FT) along indirect or direct dimensions in multidimensional NMR datasets. In its most basic form, the covariance transform applied to a homonuclear 2D NMR data set, such as a total correlation spectroscopy (TOCSY)[4] or nuclear Overhauser enhancement spectroscopy (NOESY)[5] data set, endows the indirect dimension with the same high resolution as the direct dimension and thereby enhances the spectral resolution, reduces the experimental NMR time, or both. Over the recent past, the principles of covariance NMR have been extended and applied to different types of NMR datasets, including heteronuclear 2D NMR spectra[6,17] and 4D NMR spectra.[7] The following sections describe both the principles and selected applications of covariance NMR.

7.2 DIRECT COVARIANCE NMR

Covariance NMR utilizes the correspondence between physical correlations between magnetic spins and statistical covariances contained in a set of 1D NMR spectra belonging to different spin evolution times.[1] Such a set is typically collected using the canonical 2D NMR scheme (see Chapters 1 and 2), "Preparation – Evolution (t_1) – Mixing (τ_m) – Detection (t_2)",[8] although alternative schemes are conceivable. After Fourier transformation along the detection dimension t_2, the digitized input data can then be represented

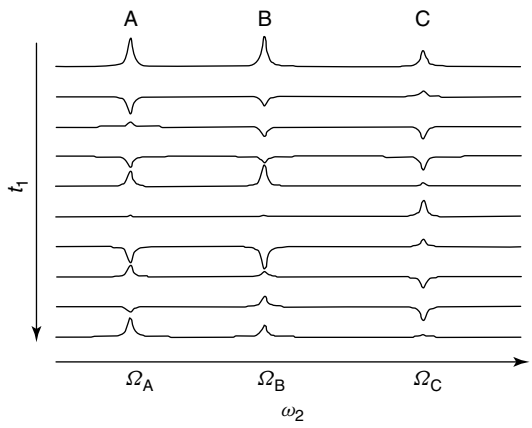

Figure 7.1. An example of a mixed time-frequency matrix $\boldsymbol{S}(t_1,\omega_2)$ with 10 t_1 increments ($N_1 = 10$) for a NOESY experiment of a three-spin 1/2 system where spins A and B undergo cross relaxation and spin C does not.

as a mixed time–frequency $N_1 \times N_2$ matrix $\boldsymbol{S}$, where element S_{ij} belongs to the bivariate function $S(t_1, \omega_2)$ sampled at the ith t_1 increment and at the jth frequency point ω_2. An example of a mixed-time frequency matrix $\boldsymbol{S}$ is shown in Figure 7.1 for a NOESY experiment of an ABC three-spin system, where all three spins are weakly coupled and where only spins A and B undergo cross relaxation.

Spin correlation information can be obtained in the following way. Consider two spins A and B with chemical shifts Ω_A and Ω_B respectively. If spins A and B exchange magnetization during the mixing period of the 2D experiment, the resonances of spins A and B are generally modulated as a function of t_1 in a manner such that they have a nonvanishing covariance, i.e.,

$$C_{AB}^2 = \frac{1}{t_{1,\max}} \int_0^{t_{1,\max}} S(t_1, \Omega_A) \cdot S(t_1, \Omega_B) \mathrm{d}t_1 \quad (7.1)$$

where it is assumed that axial peaks have been suppressed, i.e., $\int_0^{t_{1,\max}} S(t_1, \omega_2) \mathrm{d}t_1 = 0$ for all resonances along ω_2. Equation (7.1) describes the statistical interdependence of the amplitudes of resonances of spins A and B over evolution time t_1. Figure 7.2 shows correlation (scatter) plots between the peak intensities of spins A and B (Figure 7.2a,c,e) and spins A and C (Figure 7.2b,d,f) for 289 t_1 increments, for three different mixing times τ_m. To each correlation plot a Pearson correlation coefficient R can be assigned, which is a normalized covariance, e.g., $R_{AB} = C_{AB}^2 / (C_{AA}^2 C_{BB}^2)^{1/2}$ for Figure 7.2(a), (c), and (e). The correlation coefficients are zero for the rectangular distribution of Figure 7.2(a) and (b), because $\tau_m = 0$, and Figure 7.2(d) and (f), because there is no nuclear Overhauser enhancement (NOE) between spins A and C. In Figure 7.2(c) and (e), the exchange of magnetization between spins A and B causes the intensity correlations to take the shape of parallelograms, and therefore to give correlation coefficients $R \neq 0$.

Matrix notation provides a compact representation of all possible covariances between all resonances (or columns) of matrix $\boldsymbol{S}$:

$$\boldsymbol{C}^2 = \boldsymbol{S}^{\mathrm{T}} \boldsymbol{S} / N_1 \quad (7.2)$$

where superscript T denotes the matrix transpose. Because only the relative and not the absolute intensities are relevant, division by N_1 can often be discarded.

Under idealized circumstances, the spin correlation information obtained by 2D FT and covariance NMR is essentially identical, which can be seen as follows. Let $F(\omega_1, \omega_2)$ denote the FT along t_1 of $S(t_1, \omega_2)$. Then the integral of the product of $S(t_1, \Omega_A)$ and $S(t_1, \Omega_B)$ along t_1 is, up to a constant prefactor, equal to the integral of the product of $F(\omega_1, \Omega_A)$ and $F(\omega_1, \Omega_B)$ along ω_1 by Parseval's theorem, which follows from the unitary property of FT and which is a generalization of the power theorem of Fourier theory.[2,9] Expression of this relationship in matrix notation yields the covariance spectrum

$$\boldsymbol{C}^2 \propto \boldsymbol{S}^{\mathrm{T}} \boldsymbol{S} \propto \boldsymbol{F}^{\mathrm{T}} \boldsymbol{F} \quad (7.3)$$

where $\boldsymbol{F}$ is the 2D FT spectrum obtained from $\boldsymbol{S}$ by application of the FT along each t_1 column. If the number of recorded t_1 points, N_1, is small compared to N_2, $\boldsymbol{F}$ is not symmetric, independent of zero-filling. On the other hand, the direct covariance spectrum $\boldsymbol{C}^2$ calculated according to equation (7.3) is a symmetric $N_2 \times N_2$ matrix with a resolution along both dimensions that corresponds to the resolution of $\boldsymbol{F}$ along the ω_2 dimension.

The matrix square root of $\boldsymbol{C}^2$ permits the reconstruction of an idealized phase-sensitive 2D FT spectrum of $\boldsymbol{F}$, $\boldsymbol{F}_{\mathrm{ideal}}$, which has the same high spectral resolution along both frequency domains[2,3]

$$\boldsymbol{C} = (\boldsymbol{C}^2)^{1/2} \propto (\boldsymbol{S}^{\mathrm{T}} \boldsymbol{S})^{1/2} \propto (\boldsymbol{F}^{\mathrm{T}} \boldsymbol{F})^{1/2} \cong \boldsymbol{F}_{\mathrm{ideal}} \quad (7.4)$$

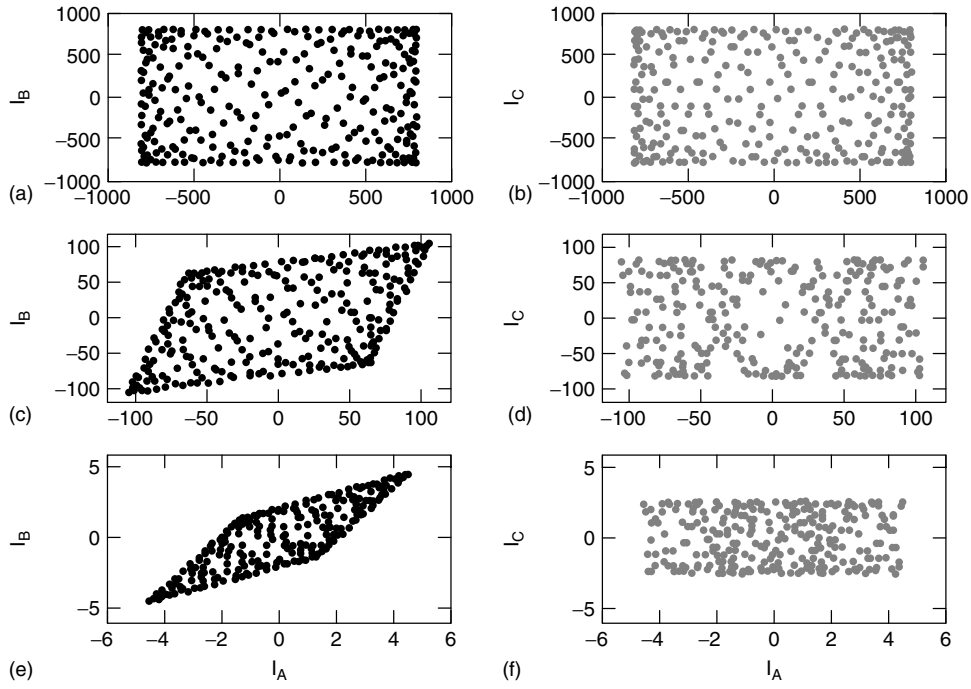

Figure 7.2. Correlation plots of 1D peak amplitudes over a set of 289 t_1 increments of mixed-time frequency data set of a simulated NOESY experiment of three-spin 1/2 system of Figure 7.1. Each circle corresponds to a different t_1 increment. Left panels give correlations between spin A and spin B for different mixing times $\tau_m = 0$ (a), $\tau_m = T$ (c), and $\tau_m = 2T$ (e). Right panels give correlations between spin A and spin C for mixing times $\tau_m = 0$ (b), $\tau_m = T$ (d), and $\tau_m = 2T$ (f). Communication between spin pairs by means of cross relaxation during the NOESY mixing time leads to skewed *xy* distributions and thereby to nonvanishing covariances and correlation coefficients. The correlation coefficients *R* are as follows: 0.001 (a), 0.009 (b), 0.46 (c), 0.007 (d), 0.76 (e), 0.008 (f).

Covariance NMR does not require $\boldsymbol{F}$ to be phase corrected along the indirect dimension ω_1. Figure 7.3 shows the covariance spectrum calculated according to equation (7.4) from the three-spin NOESY matrix $\boldsymbol{S}$ of Figure 7.1. The spectrum is fully symmetric with diagonal peaks and cross peaks at the expected positions, namely between spins A and B, but not between spins A and C or spins B and C.

The matrix square root discriminates between the different mechanisms that can give rise to a nonzero covariance between two resonances Ω_A and Ω_B, such as when both spins exchange magnetization with a third spin, leading to spin diffusion, or when they exchange magnetization with two different spins that spectrally overlap. The former case gives rise to relay peaks and the latter to pseudo-relay peaks. The matrix square root in equation (7.4) is analogous to halving the mixing time to minimize relay effects in a NOESY spectrum.[2]

The ability of direct covariance NMR to reconstruct an $N_2 \times N_2$ spectrum from an $N_1 \times N_2$ spectrum with $N_1 < N_2$ suggests that direct covariance provides an effective method for resolution enhancement along the indirect dimension.[3,10] This is in fact the case, as is illustrated in Figure 7.4 for a TOCSY spectrum of the cyclic decapeptide antamanide. In a study that explored the minimal number of t_1-increments required, a TOCSY spectrum with only 48 t_1-increments was shown to produce an accurate reconstruction of the target TOCSY spectrum with over 1024 t_1-increments, after regions with high statistical uncertainties were masked.[10] The covariance principles described here can also be fruitfully applied to NMR spectra of solids.[11–13]

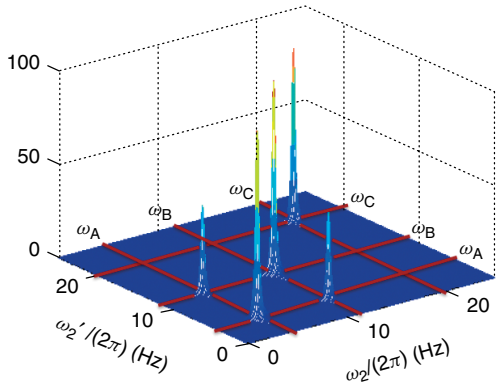

Figure 7.3. Covariance spectrum $\boldsymbol{C}$ calculated according to equation 7.4 from the three-spin NOESY matrix $\boldsymbol{S}$ of Figure 7.1. The spectrum is fully symmetric with the three diagonal peaks and two cross peaks at the expected positions between spins A and B.

7.3 COMPUTATIONAL ASPECTS

The computationally efficient implementation of the matrix square root is critical for practical applications of the covariance method. The matrix square root of a symmetric matrix $\boldsymbol{A}$, i.e., the positive semidefinite matrix $\boldsymbol{X}$ satisfying $\boldsymbol{X}^2 = \boldsymbol{A}$, can be calculated from the eigendecomposition of $\boldsymbol{A} = \boldsymbol{E}\boldsymbol{\Lambda}\boldsymbol{E}^{-1}$ and hence $\boldsymbol{X} = \boldsymbol{E}\boldsymbol{\Lambda}^{1/2}\boldsymbol{E}^{-1}$, where $\boldsymbol{E}$ contains the eigenvectors of $\boldsymbol{A}$ as its columns. $\boldsymbol{\Lambda}$ is a diagonal matrix with the eigenvalues on its diagonal and the matrix square root of $\boldsymbol{\Lambda}$ is its element-by-element square root.

By taking into account the covariance structure of $\boldsymbol{S}^{\mathrm{T}}\boldsymbol{S}$, it is often possible to speed up the computation substantially by means of singular value decomposition (SVD) of $\boldsymbol{S}^{\mathrm{T}}$ itself.[3] SVD decomposes the $N_2 \times N_1$ matrix $\boldsymbol{S}^{\mathrm{T}}$ into the product of three matrices $\boldsymbol{S}^{\mathrm{T}} = \boldsymbol{U}\cdot\boldsymbol{W}\cdot\boldsymbol{V}^{\mathrm{T}}$, where $\boldsymbol{U}$ and $\boldsymbol{V}$ are orthogonal and $\boldsymbol{W}$ is a diagonal matrix with positive entries or zeros. Substitution of $\boldsymbol{S}^{\mathrm{T}}$ by its SVD yields

$$\begin{aligned}\boldsymbol{S}^{\mathrm{T}}\boldsymbol{S} &= \boldsymbol{U}\boldsymbol{W}\boldsymbol{V}^{\mathrm{T}}\cdot(\boldsymbol{U}\boldsymbol{W}\boldsymbol{V}^{\mathrm{T}})^{\mathrm{T}} \\ &= \boldsymbol{U}\boldsymbol{W}\boldsymbol{V}^{\mathrm{T}}\boldsymbol{V}\boldsymbol{W}\boldsymbol{U}^{\mathrm{T}} = \boldsymbol{U}\boldsymbol{W}^2\boldsymbol{U}^{\mathrm{T}}\end{aligned} \qquad (7.5)$$

which is equivalent to the matrix diagonalization of $\boldsymbol{S}^{\mathrm{T}}\boldsymbol{S}$ with eigenvalues that are the squares of the singular values. It directly follows for the square root matrix

$$\boldsymbol{C} = (\boldsymbol{S}^{\mathrm{T}}\boldsymbol{S})^{1/2} = \boldsymbol{U}\cdot\boldsymbol{W}\cdot\boldsymbol{U}^{\mathrm{T}} \qquad (7.6)$$

When $N_1 \ll N_2$, which is often the case in practice, SVD affords a substantial speedup over matrix diagonalization.[3] Moreover, SVD implementation enables covariance processing of 4D NMR spectra (vide infra).

Covariance NMR transforms an experimental 2D NMR dataset to a symmetric, positive semidefinite spectrum. This implicitly assumes that the idealized 2D FT-type spectrum to be reconstructed is also positive semidefinite. This is indeed the case for many 2D experiments, such as NOESY, where the amplitudes of the diagonal peaks dominate those of the cross peaks. For other experiments, situations exist where this is not the case, such as for a TOCSY of a two-spin system with a mixing time $\tau_{\mathrm{m}} = 1/(4J)$ where J is the scalar J-coupling (in Hz) between the two spins. In this case, the diagonal peaks of the 2D FT spectrum are zero, while the cross peaks are nonzero and the corresponding covariance spectrum $\boldsymbol{C} = (\boldsymbol{F}^{\mathrm{T}}\boldsymbol{F})^{1/2}$ is diagonal. To remedy this problem, the 2D FT spectrum $\boldsymbol{F}$ can be regularized by adding a properly scaled unit matrix to $\boldsymbol{F}$ prior to the covariance transformation, which is followed by subtraction of the same unit matrix from the output covariance matrix $\boldsymbol{C}$.[14]

7.4 4D COVARIANCE NMR

The ability to apply covariance NMR to frequency domain data sets (equation (7.4)) allows for the correction of baseline artifacts including ridges prior to covariance transformation, which is particularly useful for the application of covariance NMR to 4D data sets. Key to the extension of covariance NMR to four dimensions is the representation of a 4D dataset as a 2D data array or matrix. Consider a 4D spectrum $F(\omega_1, \omega_2, \omega_3, \omega_4)$, where $\omega_1, \ldots, \omega_4$ range over $N_1, \ldots, N_4$ discrete frequency increments. Let I be an index ranging over the $N_1 \times N_2$ donor frequency pairs (ω_1, ω_2) and J ranging over the $N_3 \times N_4$ acceptor frequency pairs (ω_3, ω_4). Then $F(\omega_1, \omega_2, \omega_3, \omega_4)$ can be represented by a matrix $\boldsymbol{F}$ with elements F_{IJ}. Provided that the 4D spectrum reflects symmetric spin-magnetization transfers with respect to donor and acceptor planes, as is the case, e.g., in a 4D ^{13}C-edited NOESY, a covariance transform yields a resolution-enhanced $N_3 \times N_4 \times N_3 \times N_4$ spectrum by mapping the higher resolution of the acceptor planes onto the donor planes.[7]

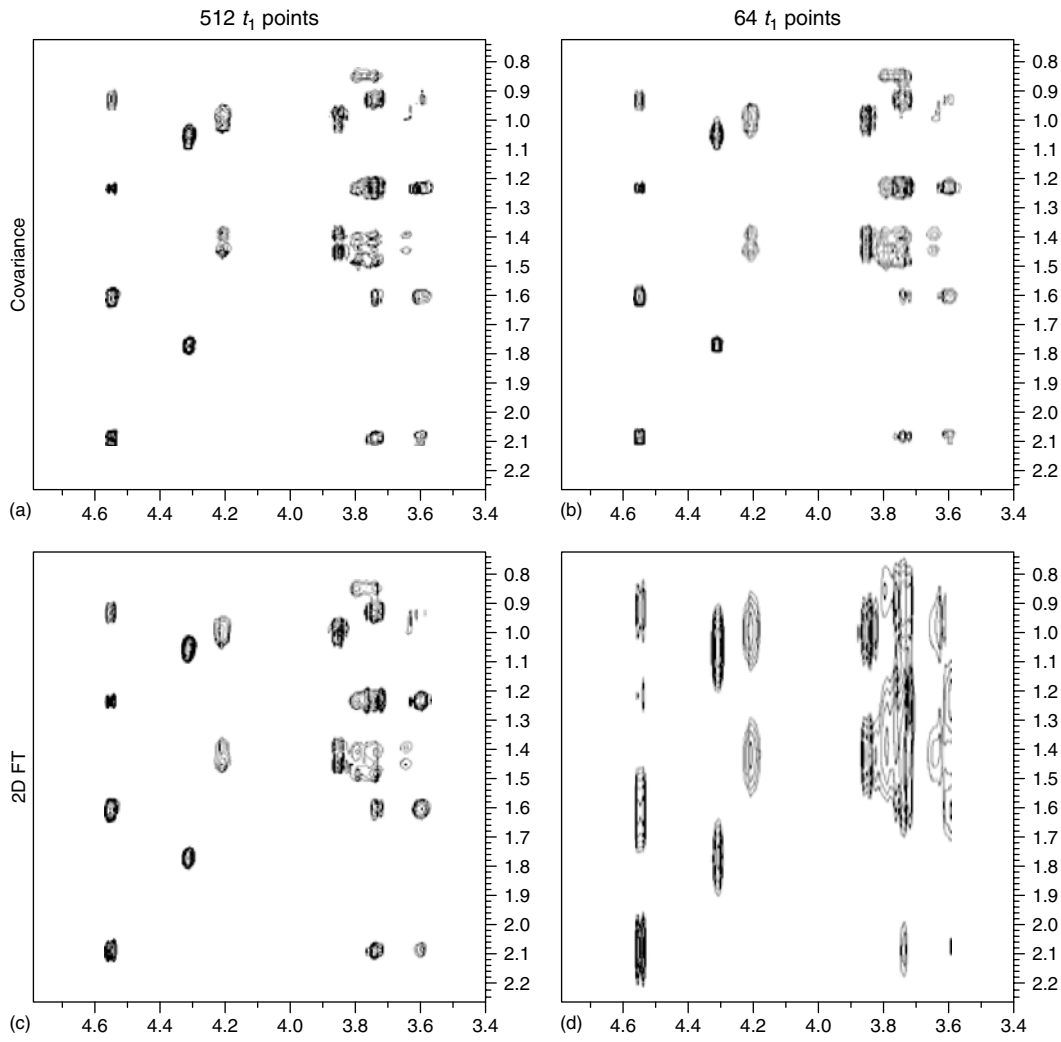

Figure 7.4. Comparison of experimental covariance TOCSY spectra (a,b) with corresponding 2D FT spectra (c,d) of cyclic decapeptide antamanide for 512 (a,c), and 64 (b,d) t_1 increments, respectively. Covariance spectrum (b) demonstrates the degree of resolution enhancement achievable along the indirect dimension using a limited number of t_1 increments.

Covariance NMR can also be applied to spectra that are inherently asymmetric, such as 4D $^{13}C-^{15}N$-edited NOESY spectra, by embedding such spectra in larger, symmetric spectra, for instance by using $^{13}C-^{15}N$-edited, ^{15}N-edited, $^{15}N-^{13}C$-edited, and ^{13}C-edited NOESY spectra as subspectra. Shared-evolution methodology enables all four subspectra to be collected in a single experiment that requires the same amount of measurement time as for a single subspectrum.[15] For this type of spectrum, 4D covariance NMR provides 20- to 30-fold resolution enhancement along a given donor dimension (Figure 7.5).[7,15] The gain in resolution greatly enhances the analysis of 4D NOESY spectra by resolving more cross peaks. This leads to additional long-range and stereospecific distance constraints,[16] both of which can result in improved protein structure determination not readily achievable by other means.

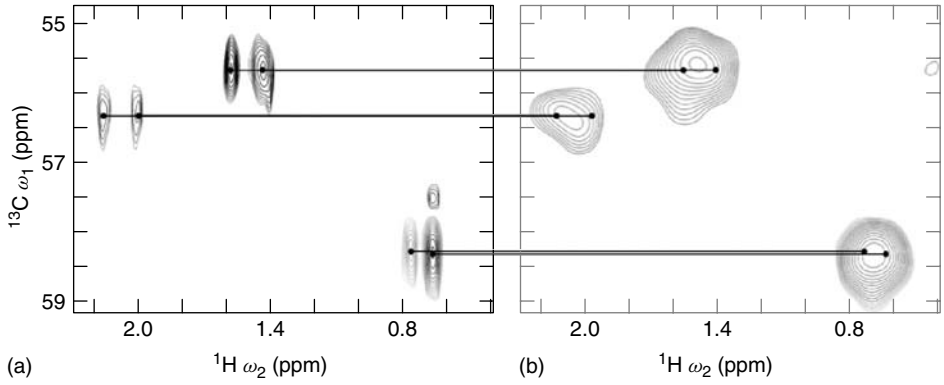

Figure 7.5. Portion of the Q70 N–H plane (^{15}N chemical shift 125.6 ppm, ^{1}H chemical shift 7.80 ppm) of (a) 4D covariance NOESY of the 24 kDa protein DdCAD-1 calculated from (b) 4D FT spectrum acquired using shared evolution,[15] illustrating how the covariance transform resolves peaks that cannot be separated in the FT spectrum.[16]

7.5 INDIRECT COVARIANCE NMR

From the definition of a direct covariance spectrum described in equation (7.4), it is possible to interchange formally the roles of $\boldsymbol{F}$ and $\boldsymbol{F}^{\mathrm{T}}$, which leads to an "indirect" covariance NMR spectrum:[17]

$$\boldsymbol{C}_{\text{indirect}} = (\boldsymbol{F} \cdot \boldsymbol{F}^{\mathrm{T}})^{1/2} \tag{7.7}$$

As a consequence, $\boldsymbol{C}_{\text{indirect}}$ is a symmetric matrix whose axes are defined by the *indirect* dimension (ω_1) of $\boldsymbol{F}$. Thus, equation (7.7) (yields a $N_1 \times N_1$ spectrum, whereas equation (7.4) yields an $N_2 \times N_2$ spectrum. Although application of equation (7.7) to a homonuclear dataset with $N_1 < N_2$ generally does not provide resolution enhancement, it can be used to suppress artifacts such as residual water and t_1 ridges.[18]

Indirect covariance produces spectra with unique features when applied to nonsymmetric NMR spectra, providing spin correlation information that would be difficult to directly obtain from 2D FT spectra. For example, indirect covariance processing of a heteronuclear ^{1}H–^{13}C HSQC-TOCSY spectrum yields a homonuclear ^{13}C–^{13}C TOCSY spectrum with the sensitivity of a proton-detected experiment.[17] Thus, indirect covariance allows for the reconstruction of ^{13}C–^{13}C correlations with the benefit of the eightfold increase in proton-detection sensitivity over carbon detection.

The concept of indirect covariance NMR has been extended by Blinov, Martin, and coworkers and by Kupče and Freeman to the reconstruction of nonsymmetric spectra from pairs of spectra $\boldsymbol{F}$ and $\boldsymbol{G}$

$$\boldsymbol{C} = \boldsymbol{F} \cdot \boldsymbol{G}^{\mathrm{T}} \tag{7.8}$$

termed unsymmetric covariance or hyperdimensional NMR respectively.[6,19,20] Because (accidental) spectral overlap in the concatenated dimension may lead to false peaks in the resulting unsymmetric covariance spectrum, this approach works best when applied either to relatively small molecular systems or to uncrowded planes of higher-dimensional spectra.

As an example, when the matrix multiplication of equation (7.8) is applied to a ^{1}H–^{13}C-HSQC spectrum and a ^{1}H–^{13}C-HMBC spectrum, it sums over the common direct ^{1}H dimensions yielding a correlation spectrum of carbon chemical shifts on the basis of J-coupling connectivities.[21] The covariance treatment thereby represents an effective alternative to the direct measurement of a homonuclear ^{13}C-detected spectrum, at significantly higher sensitivity.[6] Unsymmetric covariance NMR has proven useful in studies of small molecules.[22–24] Hyperdimensional NMR[25] and the Burrow–Owl formalism[26] extend the concepts of covariance NMR to the reconstruction of not necessarily symmetric higher-dimensional spectra of proteins from lower-dimensional spectra. The COBRA approach for backbone assignment uses covariance-based correlations to reconstruct a spectrum that sequentially links backbone amide proton–nitrogen pairs.[27]

In FT NMR, signal-to-noise (S/N) ratios provide a convenient statistic for evaluating the sensitivity of a spectrum by comparison of signal intensities

to a (mostly) uniform noise floor. Unlike FT, the covariance transform of equation (7.8) is a nonlinear processing method, which renders the noise floor of a spectrum nonuniform. In this case, sensitivity estimates (e.g., from S/N ratios comparing signal intensities to signal-free baseline regions) either under- or overestimate the sensitivity of the nonlinearly processed spectrum.[28,29] The recently introduced $\boldsymbol{Z}$-matrix formalism[29] converts the indirect covariance spectrum $\boldsymbol{C}$ of equation (7.8) into one that has a uniform noise floor that lends itself to the same type of sensitivity analysis as a 2D FT spectrum.

7.6 OTHER STATISTICAL SPECTROSCOPY APPROACHES

Statistical methods[30] for the analysis of correlated changes of experimental spectroscopic data have been applied in other contexts. For example, in multiphoton ionization spectroscopy, covariance mapping is applied to retrieve hidden correlations in highly fluctuating signals.[31] Stoyanova and Brown applied covariance processing and principal component analysis (PCA) for the automatic quantification of individual resonances.[32,33] In generalized two-dimensional (GEN2D) spectroscopy, Noda introduced statistical correlation analysis of optical resonances (including infrared, Raman, near-infrared, and ultraviolet) owing to changes in the experimental conditions, such as temperature and pressure.[34,35] The same concept was also applied to diffusion NMR experiments[36] as an alternative way to process diffusion-ordered spectroscopy (DOSY) spectra.[37] What distinguishes covariance NMR from these approaches is that it establishes spin correlations through magnetization or coherence transfer as an alternative route to multidimensional FT NMR.

Recently, the covariance matrices that belong to a set of 1D NMR spectra of a series of samples have been used to identify the chemical components that show the largest fluctuations by means of statistical total correlation spectroscopy (STOCSY),[38] an approach that can also be combined with mass spectrometry using statistical heterospectroscopy (SHY).[39] While formally closely related to covariance NMR, STOCSY and SHY operate on 1D datasets of physically different samples, e.g., collected from different subjects. Both STOCSY and covariance NMR have broad applicability in the emerging field of metabolomics and metabonomics.

7.7 COMPLEX MIXTURE ANALYSIS AND METABOLOMICS

The resolution and sensitivity gains afforded by covariance NMR can be leveraged into the ability to run an increased number of NMR experiments in a fixed amount of spectrometer time. This permits increased throughput that is useful, for example, in metabolomics, where large numbers of samples need to be analyzed in a timely fashion.[40] Moreover, implicit in the implementation of covariance NMR via SVD or matrix diagonalization is the representation of an NMR spectrum by the eigenvectors (principal components) of its covariance matrix. In the absence of chemical shift degeneracy, each principal component of the TOCSY spectrum of a mixed solution is the 1D spectrum for a spin system within one of the solutes in the mixture.[41] In the presence of significant peak overlaps of the different components, the deconvolution of a TOCSY spectrum of a mixture via PCA may break down. However, given that TOCSY peaks are generally positive, linear algebraic nonnegative matrix factorization (NMF) applied to covariance or 2D FT TOCSY spectra allows the rather robust deconvolution of TOCSY spectra of complex mixtures into the 1D spectra of each mixture component.[42]

Both PCA and NMF perform unsupervised clustering of cross peaks into groups that belong to individual components. Another clustering method, termed DemixC, has shown significant promise in the deconvolution of TOCSY spectra of mixtures.[43] The DemixC method uses covariance techniques to guide the clustering of slices in a TOCSY spectrum and to recognize cross sections that represent individual mixture components that are least likely to be affected by peak overlaps. DemixC and NMF can be applied not only to homonuclear TOCSY but also to ^{1}H-^{13}C-HSQC-TOCSY spectra, allowing for the identification of compounds in a mixture via the extraction of both the ^{1}H and ^{13}C 1D NMR spectra of the spin systems present.[44] DemixC traces and NMF components can then be screened, using suitable matching algorithms, against a database of 1D spectra, such as the BMRB[45] and the HMDB,[46] in order to identify the associated compounds.[47]

A suite of web servers is publicly accessible at http://spinportal.magnet.fsu.edu, called COLMAR (for complex mixture analysis by NMR), to facilitate the above-described processing, analysis, and interpretation of metabolomics data. *COLMAR covariance* uploads 2D data sets in various formats and

returns the covariance spectrum, *COLMAR DemixC* deconvolutes the TOCSY spectrum, and *COLMAR query* screens the DemixC traces against a selected metabolite database (BMRB or HMDB). Studies of the venom of a single walking stick insect[48] and of a cancer cell extract[44] testify to the utility of these tools in natural product analysis and metabolomics.

7.8 CONCLUSION AND OUTLOOK

Because covariance NMR allows spin correlations to be probed at spectral resolutions or sensitivities that are often not achievable via direct experimental measurements, it affords a substantial gain in the resolution obtainable within a fixed amount of measurement time, which is valuable for high-throughput applications such as the measurement of 4D spectra of proteins in the context of structural genomics projects, or the shortening of the measurement time of 2D spectra in metabolomics studies. Leveraging of these gains can be further enhanced by algorithmic developments for the automated analysis and interpretation of covariance spectra, for compound identification, spin resonance assignment, and the extraction of structural and dynamic information.

REFERENCES

1. R. Brüschweiler and F. Zhang, *J. Chem. Phys.*, 2004, **120**, 5253–5260.
2. R. Brüschweiler, *J. Chem. Phys.*, 2004, **121**, 409–414.
3. N. Trbovic, S. Smirnov, F. Zhang, and R. Brüschweiler, *J. Magn. Reson.*, 2004, **171**, 277–283.
4. L. Braunschweiler and R. R. Ernst, *J. Magn. Reson.*, 1983, **53**, 521–528.
5. J. Jeener, B. H. Meier, P. Bachmann, and R. R. Ernst, *J. Chem. Phys.*, 1979, **71**, 4546–4553.
6. K. A. Blinov, N. I. Larin, A. Williams, K. Mills, and G. E. Martin, *J. Heterocycl. Chem.*, 2006, **43**, 163–166.
7. D. A. Snyder, F. Zhang, and R. Brüschweiler, *J. Biomol. NMR*, 2007, **39**, 165–175.
8. W. P. Aue, E. Bartholdi, and R. R. Ernst, *J. Chem. Phys.*, 1976, **64**, 2229–2246.
9. P. Papoulis, *Signal Analysis*, McGraw-Hill: London, 1984.
10. Y. B. Chen, F. Zhang, W. Bermel, and R. Brüschweiler, *J. Am. Chem. Soc.*, 2006, **128**, 15564–15565.
11. C. Kaiser, J. J. Lopez, W. Bermel, and C. Glaubitz, *Biochim. Biophys. Acta*, 2007, **1768**, 3107–3115.
12. B. Hu, J. P. Amoureux, and J. Trebosc, *Solid State Nucl. Magn. Reson.*, 2007, **31**, 163–168.
13. B. Hu, J. P. Amoureux, J. Trebosc, M. Deschamps, and G. Tricot, *J. Chem. Phys.*, 2008, **128**, 134502.
14. Y. B. Chen, F. Zhang, D. A. Snyder, Z. Gan, L. Bruschweiler-Li, and R. Brüschweiler, *J. Biomol. NMR.*, 2007, **38**, 73–77.
15. Y. Xu, D. Long, and D. Yang, *J. Am. Chem. Soc.*, 2007, **129**, 7722–7723.
16. D. A. Snyder, Y. Xu, D. Yang, and R. Brüschweiler, *J. Am. Chem. Soc.*, 2007, **129**, 14126–14127.
17. F. Zhang and R. Brüschweiler, *J. Am. Chem. Soc.*, 2004, **126**, 13180–13181.
18. Y. Chen, F. Zhang, and R. Bruschweiler, *Magn. Reson. Chem.*, 2007, **45**, 925–928.
19. K. A. Blinov, A. J. Williams, B. D. Hilton, P. A. Irish, and G. E. Martin, *Magn. Reson. Chem.*, 2007, **45**, 544–546.
20. Ē. Kupče and R. Freeman, *J. Am. Chem. Soc.*, 2006, **128**, 6020–6021.
21. K. A. Blinov, N. I. Larin, A. J. Williams, M. Zell, and G. E. Martin, *Magn. Reson. Chem.*, 2006, **44**, 107–109.
22. G. E. Martin, B. D. Hilton, K. A. Blinov, and A. J. Williams, *J. Heterocycl. Chem.*, 2008, **45**, 1109–1113.
23. G. E. Martin, B. D. Hilton, P. A. Irish, K. A. Blinov, and A. J. Williams, *J. Nat. Prod.*, 2007, **70**, 1393–1396.
24. G. E. Martin, P. A. Irish, B. D. Hilton, K. A. Blinov, and A. J. Williams, *Magn. Reson. Chem.*, 2007, **45**, 624–627.
25. Ē. Kupče and R. Freeman, *Prog. NMR Spectrosc.*, 2008, **52**, 22–30.
26. G. Benison, D. S. Berkholz, and E. Barbar, *J. Magn. Reson.*, 2007, **189**, 173–181.
27. E. Lescop and B. Brutscher, *J. Am. Chem. Soc.*, 2007, **129**, 11916–11917.
28. D. L. Donoho, I. M. Johnstone, A. S. Stern, and J. C. Hoch, *Proc. Natl. Acad. Sci. USA*, 1990, **87**, 5066–5068.
29. D. A. Snyder, A. Ghosh, F. Zhang, T. Szyperski, and R. Brüschweiler, *J. Chem. Phys.*, 2008, **129**, 104511.

30. A. J. Johnson and D. W. Wichern, *Applied Multivariate Statistical Analysis*, Prentice Hall: New Jersey, Upper Saddle River, 2002.

31. L. J. Frasinski, K. Codling, and P. A. Hatherly, *Science*, 1989, **246**, 1029–1031.

32. T. R. Brown and R. Stoyanova, *J. Magn. Reson. B*, 1996, **112**, 32–43.

33. R. Stoyanova and T. R. Brown, *J. Magn. Reson.*, 2002, **154**, 163–175.

34. I. Noda, *J. Am. Chem. Soc.*, 1989, **111**, 8116–8118.

35. I. Noda, A. E. Dowrey, C. Marcott, G. M. Story, and Y. Ozaki, *Appl. Spectrosc.*, 2000, **54**, 236A–248A.

36. C. D. Eads and I. Noda, *J. Am. Chem. Soc.*, 2002, **124**, 1111–1118.

37. C. S. Johnson, *Prog. Nucl. Magn. Reson. Spectrosc.*, 1999, **34**, 203–256.

38. O. Cloarec, M. E. Dumas, A. Craig, R. H. Barton, J. Trygg, J. Hudson, C. Blancher, D. Gauguier, J. C. Lindon, E. Holmes, and J. Nicholson, *Anal. Chem.*, 2005, **77**, 1282–1289.

39. D. J. Crockford, E. Holmes, J. C. Lindon, R. S. Plumb, S. Zirah, S. J. Bruce, P. Rainville, C. L. Stumpf, and J. K. Nicholson, *Anal. Chem.*, 2006, **78**, 363–371.

40. E. M. Lenz and I. D. Wilson, *J. Proteome Res.*, 2007, **6**, 443–458.

41. F. Zhang, and R. Brüschweiler, *Chemphyschem*, 2004, **5**, 794–796.

42. D. A. Snyder, F. Zhang, S. L. Robinette, L. Bruschweiler-Li, and R. Brüschweiler, *J. Chem. Phys.*, 2008, **128**, 052313.

43. F. Zhang and R. Brüschweiler, *Angew. Chem. Int. Ed.*, 2007, **46**, 2639–2642.

44. F. Zhang, L. Bruschweiler-Li, S. L. Robinette, and R. Brüschweiler, *Anal. Chem.*, 2008, **80**, 7549–7553.

45. E. L. Ulrich, H. Akutsu, J. F. Doreleijers, Y. Harano, Y. E. Ioannidis, J. Lin, M. Livny, S. Mading, D. Maziuk, Z. Miller, E. Nakatani, C. F. Schulte, D. E. Tolmie, R. K. Wenger, H. Y. Yao, and J. L. Markley, *Nucl. Acids Res.*, 2008, **36**, D402–D408.

46. D. S. Wishart, C. Knox, A. C. Guo, R. Eisner, N. Young, B. Gautam, D. D. Hau, N. Psychogios, E. Dong, S. Bouatra, R. Mandal, I. Sinelnikov, J. Xia, L. Jia, J. A. Cruz, E. Lim, C. A. Sobsey, S. Shrivastava, P. Huang, P. Liu, L. Fang, J. Peng, R. Fradette, D. Cheng, D. Tzur, M. Clements, A. Lewis, A. De Souza, A. Zuniga, M. Dawe, Y. Xiong, D. Clive, R. Greiner, A. Nazyrova, R. Shaykhutdinov, L. Li, H. J. Vogel, and I. Forsythe, *Nucl. Acids Res.*, 2007, **35**, D521–D526.

47. S. L. Robinette, F. Zhang, L. Bruschweiler-Li, and R. Brüschweiler, *Anal. Chem.*, 2008, **80**, 3606–3611.

48. F. Zhang, A. T. Dossey, C. Zachariah, A. S. Edison, and R. Bruschweiler, *Anal. Chem.*, 2007, **79**, 7748–7752.